Available online at www.sciencedirect.com
SCIENCE DIRECT
Journal of Photochemistry and Photobiology A: Chemistry 179 (2006) 81–86
Journal of Photochemistry and Photobiology A:Chemistry
www.elsevier.com/locate/jphotochem

Enhanced photoelectrochemical performance of ZnO electrodes sensitized with N-719

Keita Kakiuchi, Eiji Hosono, Shinobu Fujihara *

Department of Applied Chemistry, Faculty of Science and Technology, Keio University, 3-14-1 Hiyoshi, Kohoku-ku, Yokohama 223-8522, Japan

Received 4 April 2005; received in revised form 10 June 2005; accepted 22 July 2005
Available online 26 August 2005

Abstract

To improve dye-loading in photoanodes, microstructure of ZnO films was modified through the formation and pyrolysis of layered hydroxide zinc acetate (LHZA) grown in a methanolic solution of zinc acetate dihydrate. Appropriate annealing treatments for the films led to the formation of mesoporous microstructure with an average pore diameter of 12 nm. It was demonstrated that loading of N-719 in the ZnO films was successful without influence of protons in solutions, as evidenced by a large dye amount of 1.4×10^{-7} mol/cm^2, and hence a high short-circuit photocurrent density of 12.6 mA/cm^2. Sandwich-type dye-sensitized solar cells using the present ZnO/N-719 photoanode exhibited a conversion efficiency as high as 4.1% (AM-1.5, 100 mW/cm^2).

Keywords: Dye-sensitized solar cells; Zinc oxide; Microstructure; N-719; Conversion efficiency

1. Introduction

Nanoparticulate porous titanium dioxide (TiO_2) films were found to be useful as photoanodes for dye-sensitized solar cells (DSCs) [1]. Among other candidates for photoanode materials, zinc oxide (ZnO) has been expected to be comparable to TiO_2 because of its higher electronic mobility and similar energy level of the conduction band. However, overall light to electricity conversion efficiencies (η) of ZnO-based cells have been inferior to those of TiO_2-based cells. In full sunlight (air mass 1.5, 100 mW/cm^2) measurements, the highest η value reported so far is 2.4% in a DSC using ZnO/eosin Y electrodes [2,3]. These results are contrary to our high expectation to ZnO enhanced by recent theoretical reports. That is, there is no clear difference in electron transfer processes from excited dyes to the semiconductor electrodes between ZnO and TiO_2, when using a ruthenium (Ru) complex of N-719 ($RuL_2(NCS)_2$:2TBA; L = 2,2′-bipyridyl-4,4′-dicarboxylic acid and TBA = tetrabutylammonium). Moreover, electron injection efficiency of ZnO is almost equivalent to that of TiO_2 [4,5].

It is believed that there is a serious problem for dye-loading of ZnO with Ru-complexes, such as N-3 and N-719 [6]. Protons derived from the Ru-complexes make the dye-loading solution relatively acidic and dissolve ZnO, generating Zn^{2+}/dye aggregates [7]. Such aggregates are harmful to the cells because they lower electron injection efficiencies and fill nano-scale pores of the ZnO photoanodes. Keis et al. [3] has overcome this problem by adding base (KOH) to the dye-loading solution and shortening the loading time. We believe that microstructures of ZnO films used as photoanodes should be modified more precisely to improve the cell performance [8]. In this view, micrometer-scale as well as nanometer-scale porous ZnO films will find a particularly important role. Whereas nanometer-scale pores (mesopores) contribute to an extraordinary increase of dye-adsorption sites in number, micrometer-scale pores facilitate mass transfer of electrolytes to dyed ZnO surfaces. However, not only traditional techniques, such as screen printing and doctor blading but also novel methods based on electrodeposition and spray coating have not allowed us to

* Corresponding author. Tel.: +81 45 566 1581; fax: +81 45 566 1551.
E-mail address: shinobu@applc.keio.ac.jp (S. Fujihara).

1010-6030/$ – see front matter © 2005 Elsevier B.V. All rights reserved.
doi:10.1016/j.jphotochem.2005.07.018

produce such microstructures [3,9–11]. We then report here a new nanostructure of ZnO films consisting of mesoporous sheets separated from each other in a micrometer order. We also show that this nanostructure is suitable for photoanodes in DSCs having η values as high as 4.1% under the AM-1.5 illumination at 100 mW/cm^2 (1 sun).

2. Experimental procedure

2.1. Preparation of ZnO films

Zinc acetate dihydrate ($Zn(CH_3COO)_2{\cdot}2H_2O$) with 99.9% purity was obtained from Wako Pure Chemicals Co. Ltd., Japan. Anhydrous methanol was used as received from Taisei Chemical Co. Ltd., Japan, without further purification. Glass substrates coated with an indium tin oxide (ITO) electrode with a sheet resistance of 4 Ω/square were obtained from Nippon Sheet Glass Co. Ltd., Japan. ZnO films were fabricated through our original method based on a chemical bath deposition (CBD) of layered hydroxide zinc acetate (LHZA; $Zn_5(OH)_8(CH_3COO)_2{\cdot}2H_2O$) and its pyrolysis at low temperatures [12]. A solution for a CBD process was prepared by dissolving $Zn(CH_3COO)_2{\cdot}2H_2O$ (0.15 M) in methanol. The substrates were then immersed in the solution and kept at 60 °C for 30 h in a constant-temperature oven. During this procedure, LHZA films were deposited on the substrates through heterogeneous nucleation. The resultant films were rinsed with ethanol and dried sufficiently at room temperature. Subsequent heating procedures were different from those adopted in our previous work [12]. The acetate groups tend to remain in the pyrolysed ZnO films when they are heated rapidly and directly in the furnace. In the present case, therefore, the LHZA films were first heated at a low temperature of 200 °C for 5 min in air to promote pyrolysis into wurtzite-type ZnO. The ZnO films obtained were then heated at a higher temperature of 300 or 450 °C for 10 min in air, followed by quenching, to remove the acetate groups and develop the interconnection between ZnO grains.

2.2. Characterization of films

X-ray diffraction (XRD) patterns of the LHZA and the ZnO films were taken with a Rigaku RAD-C diffractometer using Cu Kα radiation. The film morphology was observed by field-emission scanning electron microscopy (FE-SEM) and transmission electron microscopy (TEM) with a Hitachi S-4700 and a Philips TECNAI F20 microscope, respectively. The specific surface area was estimated by the Brunauer–Emmett–Teller (BET) method based on the nitrogen adsorption isotherm (77 K) with a Shimadzu Tristar 3000 Micrometrics analyzer. Pore size distribution was also analyzed with the same apparatus. The Barret–Joyner–Halenda (BJH) method was applied to the adsorption branch of adsorption–desorption isotherms. X-ray photoelectron spectroscopy (XPS) was carried out using Mg Kα radiation with a JEOL JSP-9000MX.

2.3. Photoelectrochemical measurements

Dye-loading of the ZnO film was performed by immersing it in a 0.3 mM ethanolic solution of N-719 (Solaronix S.A., Switzerland) at 80 °C for typically 3 h. The dyed ZnO film was then immersed in ethanol for more than 1 h to remove dyes remained unadsorbed on the film. The amount of adsorbed dye was determined as follows. The dye was desorbed from the film by immersing in a 1 M NaOH water–ethanol (with volume ratio of 1:1) solution. The solution was then analyzed with a Hitachi U-3300 UV–vis spectrophotometer. An absorption spectrum measured was calibrated with standard solutions of N-719.

The ZnO/N-719 electrode, thus, fabricated was examined by the UV–vis spectroscopy to obtain an absorption spectrum. The electrode was then assembled into a sandwich-type open cell using platinum as a counter electrode. Both the electrodes were spaced by Parafilms^{TM} 120 μm in thickness and pressed by clamps. An electrolyte solution, which was composed of 0.1 M LiI (Wako), 0.6 M dimethylpropylimidazolium iodide (Shikoku Chemicals Co. Ltd., Japan), 0.05 M I_2 (Kanto Kagaku Co. Ltd., Japan), 1.0 M butylpyridine and 3-methoxypropionitrile (Wako), was introduced into the clamped electrodes by the capillary action.

Photocurrent (I) and photovoltage (V) of the cell were measured with an active area of 0.25 cm^2 using a commercial "I–V curve tracer" (EKO Instruments Co. Ltd., Japan; model MP-160) and simulated sunlight at AM-1.5. A 500 W (Ushio UXL-500SX) and a 150 W (Oriel Solar Simulator) Xe lamp were used for high and low power light source, respectively. An AM-1.5 filter, a water filter, and an infrared cut filter (Hoya S76-HA50) were placed in the light path to regulate light in the wavelength range of 300–800 nm. Spectral irradiance of the lamps was measured with a spectroradiometer (Ushio USR-40D). The standard data of solar (AM-1.5) spectral irradiance integrated in the 200–800 nm region was found to correspond to 59% of the integrated irradiance of the lamps. Light power density was then adjusted to 59 mW/cm^2 to evaluate the cell performance at AM-1.5 with 100 mW/cm^2. Validity of this adjustment was further confirmed by using another spectroradiometer provided by EKO Instruments (LS-100).

Photocurrent action spectra were measured under monochromatic light illumination by using a monochromator and the 500 W Xe lamp. By integrating spectral irradiance in the 400–800 nm region, light power density was estimated to be 79 mW/cm^2. The ZnO/N-719 photoanodes were illuminated through the glass substrate in all photoelectrochemical measurements. The results are not corrected with respect to transmission losses in the ITO-coated glass substrate.

3. Results and discussion

The LHZA films grew on the substrates with a unique morphology reflecting a two-dimensional crystal structure and

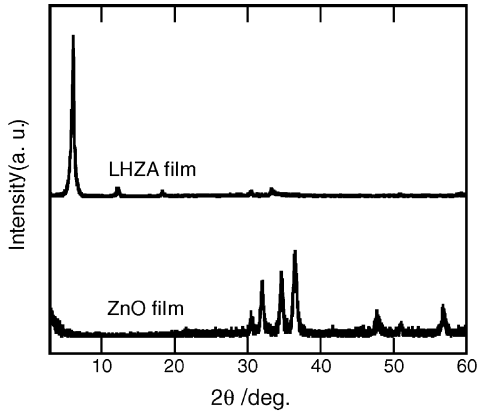

Fig. 1. XRD patterns of the LHZA film deposited in the methanolic solution of zinc acetate dihydrate and the ZnO film converted from the LHZA by pyrolysis (200 °C; 5 min) and annealing (450 °C; 10 min).

an anisotropic grain growth [13]. Subsequently, the LHZA films were pyrolysed at 200 °C for 5 min and then annealed at 450 °C for 10 min in air followed by quenching. These heat treatments led to successful transformation of LHZA to wurtzite-type ZnO films as evidenced by XRD patterns shown in Fig. 1. Furthermore, the heat treatments did not destroy the morphology of the LHZA film. Fig. 2(a) is an FE-SEM image of the ZnO film after annealing. It can be seen that the film (approximately 20 μm in thickness) consisting of sheet-like grains covers the substrate surface continuously and homogeneously. A high magnification image (Fig. 2(b)) indicates that there are micrometer-scale spaces between sheet-like grains. The film, therefore, has a macroporous structure which is supposedly beneficial to diffusion

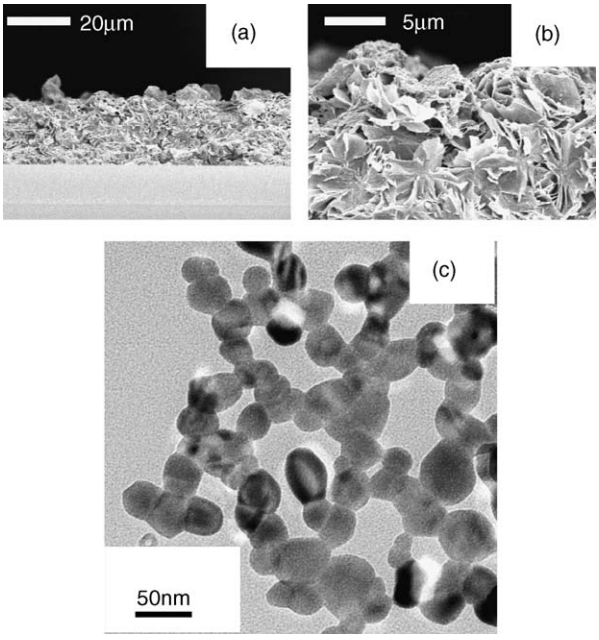

Fig. 2. (a) An FE-SEM cross-sectional image of the ZnO film. (b) An FE-SEM image of the film at high magnification. (c) A TEM image of the ZnO film.

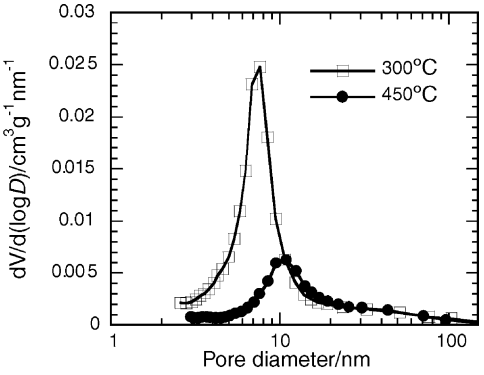

Fig. 3. Pore size distribution of the ZnO film that was annealed at 300 or 450 °C.

of dyes and electrolytes and effective scattering of incident sunlight when it is applied to photoanodes of DSCs.

The crystallite size of ZnO in the film was approximately 11 nm, as calculated from the XRD pattern (Fig. 1) using the well-known Scherrer's equation. The sheet-like grains shown in Fig. 2(b) then seem to have a polycrystalline nature. Actually, a TEM image of the sheets shown in Fig. 2(c) reveals that they are composed of nanoparticles that connect with each other, thereby implying good electron transfer properties. The TEM image also indicates the mesoporous structure of the sheets. A BET surface area was measured to be 25 m^2/g using the nitrogen sorption method. An average pore size was estimated to be 12 nm with a relatively narrow size distribution (Fig. 3). Such a microstructure of the ZnO film was first achieved by our careful investigation of the pyrolysis processes of LHZA into ZnO. It is known that pyrolysis of LHZA starts at temperatures of approximately 120 °C [12]. The pyrolysis temperature (200 °C) employed in the present work is therefore enough high to promote the dehydration, the release of the acetate groups, and the formation of ZnO. The duration of annealing (450 °C), which is necessary for improving crystallinity and developing interconnection, can then be shortened to typically 10 min without causing serious damage to the ITO electrode. The annealing temperature was found to affect the meso-structure of the ZnO films. When the ZnO film was annealed at 300 °C, an average pore size was less than 8 nm, as shown in Fig. 3.

As mentioned above, there has been a serious problem for dye-loading of ZnO with Ru-complexes, such as N-3 and N-719. Keis et al. [3] attempted to shorten the loading time or add base (KOH) to the dye-loading solution. As to shortening of the loading time, they examined the dependence of the cell performance at AM-1.5 with a lower light power density of 10 mW/cm^2 on the N-719 loading time. The conversion efficiencies showed the maximum value of 4.0% when the loading time was as short as 20 min. On increases the loading time to 30 min, 1 or 3 h, the conversion efficiencies decreased to 3.4, 3.3 and 2.3%. They attributed this degradation to the promotion of the dye-aggregation during the dye-loading procedure.

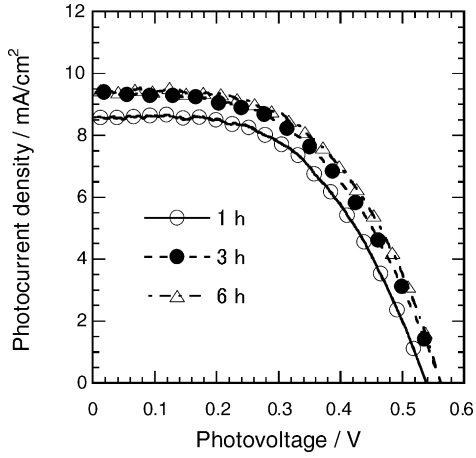

Fig. 4. *I–V* curves of the sandwich-type cell using the ZnO/N-719 photoanode; dye-loading time was varied between 1, 3 and 6 h.

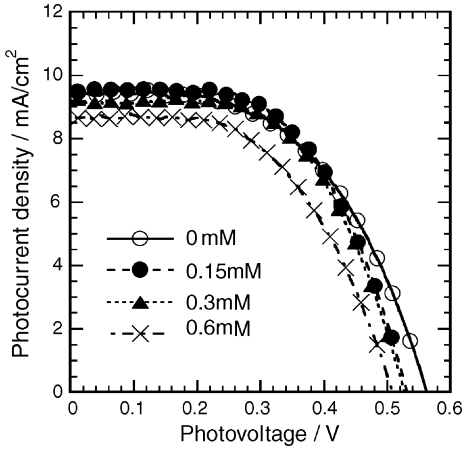

Fig. 5. *I–V* curves of the sandwich-type cell using the ZnO/N-719 photoanode; dye-loading was carried out using the N-719 solutions containing different concentrations of NaOH (0, 0.15, 0.3 and 0.6 mM).

Contrary to the results shown by Keis et al., we have found that the optimization of the microstructure of our ZnO film was also effective for improving the dye-loading procedure. Loading of N-719 to the ZnO film was carried out simply by immersing it in an ethanolic solution of N-719 (0.3 mM) at 80 °C for 3 h. Fig. 4 shows the influence of the dye-loading time on the photocurrent density–photovoltage curves of the cell with the present ZnO/N-719 photoanode under the AM-1.5 illumination at 100 mW/cm^2. The cell performance is not degraded even for the prolonged dye-loading time (6 h), indicating that the aggregation of dyes was avoided. Basically, the dye aggregates are not concentrated in the macropores of a micrometer scale. The mesopores as large as 12 nm may also help the release of the aggregates. We confirmed that the dye-loading was not successful and the cell performance could not be measured when the ZnO film annealed at 300 °C was used as the electrode. These results are contrary to those obtained for the ZnO/eosin Y systems reported previously [13]. We then need to optimize the microstructure of the photoanodes in accordance with the dyes used.

Another attempt was made to evaluate our ZnO electrodes by using the dye-loading method employed by Keis et al. [3]. Effects of the NaOH addition to the dye-loading solution was examined. Fig. 5 shows the photocurrent density–photovoltage curves of the cell using the ZnO/N-719 electrodes dyed in the solutions containing different concentrations of NaOH. Interestingly, the dye solution without adding NaOH gives the best result. With increases in the NaOH concentrations, both a short-circuit photocurrent density (J_{sc}) and an open-circuit voltage (V_{oc}) are slightly decreased. These results indicate that the present mesoporous ZnO electrodes have no dye-loading problem due to the protons of N-719. Even if the dye-aggregation occurred, the aggregates could be released from the film through the macropores.

Fig. 6(a) shows optimized photocurrent density–photovoltage curves of the cell under the AM-1.5 illumination at 100 and 14 mW/cm^2. The cell exhibits a J_{sc} value as high as 12.6 mA/cm^2 at 100 mW/cm^2. This result comes from the successful dye-loading with its amount as large as 1.4×10^{-7} mol/cm^2, which is comparable to 1.3×10^{-7} mol/cm^2 of a 10 μm thick nanoporous TiO_2 photoanode ($\eta = 10\%$) sensitized with N-3 dyes [14]. Excellent interconnection of the ZnO nanoparticles as demonstrated in Fig. 2(c) and effective light harvesting by scattering can also explain this high J_{sc} value. A V_{oc} value of 0.668 V and a fill factor (*ff*) of 0.481 gave a η value of 4.1% to this cell.

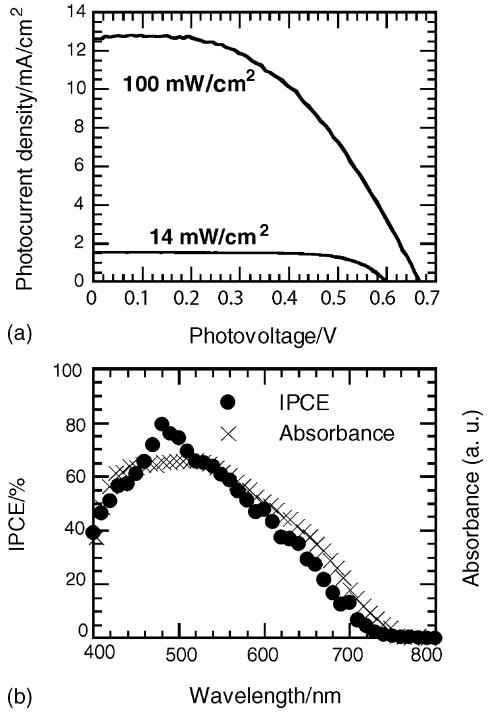

Fig. 6. (a) *I–V* curves of the sandwich-type cell using the ZnO/N-719 photoanode measured at 100 and 14 mW/cm^2. (b) A photocurrent action spectrum of the cell and an absorption spectrum of the ZnO/N-719 photoanode.

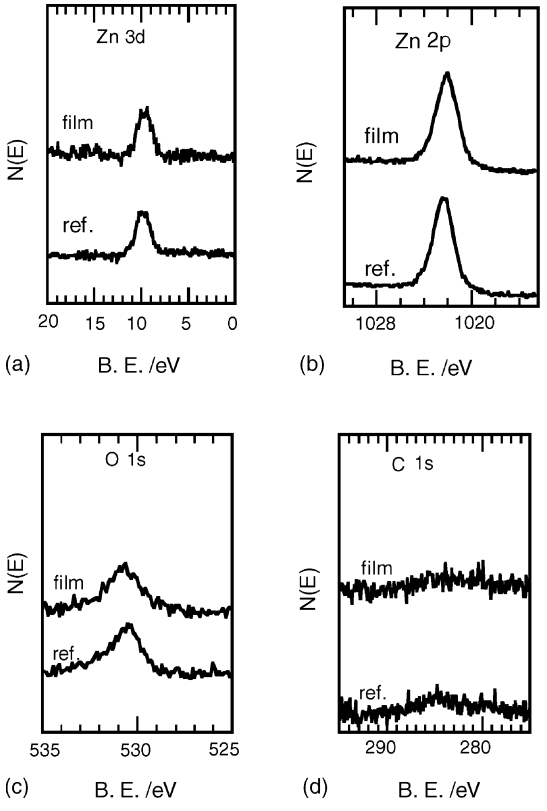

Fig. 7. XPS spectra for the ZnO film; (a) the Zn 3d, (b) the Zn 2p, (c) the O 1s, and (d) the C 1s region. A commercial ZnO powder, which was heat-treated at 450 °C for 10 min in air was used as a reference.

At a low light power density of 14 mW/cm^2, J_{sc}, V_{oc}, and *ff* were measured to be 1.5 mA/cm^2, 0.60 V, and 0.72, respectively, thereby yielding a η value of 4.6%. The fact that J_{sc} increases almost linearly upon increases in the light power density suggests that the diffusion of the electrolytes is not a rate-limiting phenomenon in our cells. Therefore, the 20 μm thick ZnO/N-719 photoanode can really work efficiently due to the macroporous structure. A photocurrent action spectrum of the cell and an absorption spectrum of the ZnO/N-719 photoanode are shown in Fig. 6(b). The maximum incident photon-to-current conversion efficiency (IPCE) exceeds 60% in the wavelength range of 460–550 nm, which corresponds to the structure of the absorption spectrum of ZnO/N-719. Taking account of the transmittance of the ITO-coated glass substrate (nearly 81%), visible light that is used for the electronic excitation of N-719 can be well converted into an electric current under the short-circuit condition.

Finally, we examined the surface of the ZnO film by XPS because there existed the possibility that the chemical modification of the surface would close recombination centers, which could be another reason for the enhanced photoelectrochemical performance of our cells. Fig. 7 shows XPS spectra of the ZnO film, which was heated at 450 °C for 10 min in air, recorded in the Zn 3d, the Zn 2p, the O 1s, and the C 1s region. Reference data are also shown in the figure. A sample for reference was prepared from a commercial ZnO powder (Sumitomo Osaka Cement Co. Ltd., Japan). The powder was heated at 450 °C for 10 min in air before the XPS measurement. In any of the spectra shown in Fig. 7, no significant difference can be seen between the film and the reference powder. Furthermore, almost no carbon species was detected in our film. Thus, we could not observe any appreciable chemical modification of the surface of the film. These results support our assertion that the microstructure of the electrode is a very important issue to be considered in fabricating DSCs.

In summary, we have experimentally demonstrated that ZnO can really be a promising alternative electrode material. A current challenge is to improve the *ff* value of the cell at the high light power density of 100 mW/cm^2. The low *ff* value implies that the recombination rate increases upon increases in the applied potential. Optimization of the cell configuration, such as electrolytes, counter electrodes, and distance between electrodes will decrease series resistance losses of the cell and increase the *ff* value.

4. Conclusions

The microstructure of the ZnO films could be controlled through the formation of LHZA and its appropriate thermal treatments. The DSC using the ZnO/N-719 photoanode exhibited the high conversion efficiency of 4.1% (AM-1.5, 100 mW/cm^2). The present experimental results support the previous theoretical works on the excellent photoelectrochemical performance of ZnO.

Acknowledgment

This work was financially supported by Amano Foundation, Shizuoka, Japan.

References

[1] B. O'Regan, M. Grätzel, Nature 353 (1991) 737–740.
[2] W.J. Lee, A. Suzuki, K. Imaeda, H. Okada, A. Wakahara, A. Yoshida, Jpn. J. Appl. Phys. Part 1 43 (2004) 152–155.
[3] K. Keis, E. Magnusson, H. Lindström, S.E. Lindquist, A. Hagfeldt, Sol. Energy Mater. Sol. Cells 73 (2002) 51–58.
In this paper, the 5% efficiency of a DSC using ZnO/N-719 was reported. However, the measurement was carried out using one-tenth (10 mW/cm^2) of the AM-1.5 (1 sun) irradiance.
[4] C. Bauer, G. Boschloo, E. Mukhtar, A. Hagfeldt, J. Phys. Chem. B 105 (2001) 5585–5588.
[5] R. Katoh, A. Furube, T. Yoshihara, K. Hara, G. Fujihashi, S. Takako, S. Murata, H. Arakawa, M. Tachiya, J. Phys. Chem. B 108 (2004) 4818–4822.
[6] "N-3" represents a ruthenium complex of $RuL_2(NCS)_2{\cdot}2H_2O$ (L = 2,2′-bipyridyl-4,4′-dicarboxylic acid).
[7] K. Keis, J. Lindgren, S.E. Lindquist, A. Hagfeldt, Langmuir 16 (2000) 4688–4694.
[8] E. Hosono, S. Fujihara, I. Honma, H. Zhou, Adv. Mater. 17 (2005) 2091–2094.

[9] J. Yamamoto, A. Tan, R. Shiratsuchi, S. Hayase, C.R. Chenthamarakshan, K. Rajeshwar, Adv. Mater. 15 (2003) 1823–1825.
[10] T. Yoshida, K. Terada, D. Schlettwein, T. Oekermann, T. Sugiura, T. Minoura, Adv. Mater. 12 (2000) 1214–1217.
[11] G.R.R.A. Kumara, K. Tennakone, I.R.M. Kottegoda, P.K.M. Bandaranayake, A. Konno, M. Okuya, S. Kaneko, K. Murakami, Semicond. Sci. Technol. 18 (2003) 312–318.
[12] E. Hosono, S. Fujihara, T. Kimura, H. Imai, J. Colloid Interface Sci. 272 (2004) 391–398.
[13] E. Hosono, S. Fujihara, T. Kimura, Electrochim. Acta 49 (2004) 2287–2293.
[14] M.K. Nazeeruddin, A. Kay, I. Rodicio, R. Humphry-Baker, E. Müller, P. Liska, N. Vlachopoulos, M. Grätzel, J. Am. Chem. Soc. 115 (1993) 6382–6390.